International Journal of Pharmaceutics 680 (2025) 125748

Contents lists available at ScienceDirect

International Journal of Pharmaceutics

journal homepage: www.elsevier.com/locate/ijpharm

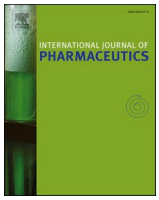

Ciprofloxacin-loaded electrosprayed lactose particles

Sai Liu, Simon Gaisford, Gareth R. Williams *

UCL School of Pharmacy, University College London, 29 – 39 Brunswick Square, London WC1N 1AX, UK

A B S T R A C T

Bacterial infections persist as a major global health challenge, underscoring the need for the development of advanced drug delivery systems. This study firstly explored the use of electrospraying to generate lactose microparticles loaded with ciprofloxacin (cipro), using polyvinyl alcohol (PVA) as an additive to enhance particle formation. Following optimization, spherical electrosprayed (ES) lactose microparticles were successfully produced with various cipro loadings (in the range of 0.25 %-1.07 % w/w). The electrosprayed particles did not contain any detectable crystalline material. Additionally, it was observed that the ES particles contained residual water, primarily originating from the production process. In terms of drug release, the ES particles exhibited rapid release kinetics within 5 h, suggesting their potential utility in treating acute bacterial infections. Notably, the formulations displayed concentration-dependent antibacterial activity against both *Staphylococcus aureus* and *Pseudomonas aeruginosa*, effectively delaying and inhibiting bacterial growth.

1. Introduction

Bacterial infections continue to represent a significant global health challenge, contributing to high morbidity and mortality (Naghavi et al., 2024). Antimicrobial resistance is projected to account for 65.9 % of deaths across all age groups by 2050 (Naghavi et al., 2024). Ciprofloxacin (cipro), a broad-spectrum fluoroquinolone antibiotic, is commonly used to treat bacterial infections due to its potent activity against both Gram-negative and Gram-positive bacteria (Kherroubi et al., 2024). However, despite its efficacy, cipro exhibits several limitations such as poor solubility and permeability, rapid clearance, and systemic side effects (Junkert et al., 2024), underscoring the need for advanced drug delivery systems.

Electrospraying (ES) has emerged as a versatile technology for producing monodisperse particles, offering significant potential for improving drug delivery (Zamani et al., 2013). Its application in antibiotic delivery represents a promising approach to treat bacterial infections (Steipel et al., 2019). Several antibiotics including ampicillin (Eltohamy et al., 2011), vancomycin, ceftazidime, and lidocaine mixtures (Hsu et al., 2018), cipro (Arauzo et al., 2021), vancomycin (Booysen et al., 2019) and azithromycin (Arauzo et al., 2021) have been successfully electrosprayed for potential use against bacterial infections. Such antibiotic-loaded particles have demonstrated positive attributes such as uniform size distribution (Nikolaou and Krasia-Christoforou, 2018), high drug loading (Landa et al., 2023), and minimum batch-to-batch variation (Ali et al., 2021).

Lactose, a biocompatible and biodegradable excipient, is widely used as a pharmaceutical carrier (Pilcer and Amighi, 2010). Several studies have explored the potential of electrospraying for fabricating lactose-based formulations (Patil et al., 2017; Cardoso et al., 2011; Amiri et al., 2021). For instance, electrosprayed formulations produced from saturated lactose solutions were found to contain both the α and β polymorphs (Patil et al., 2017). Electrohydrodynamic atomization has also been used to generate lactose crystals carrying bovine serum albumin (BSA), where BSA was adsorbed onto the lactose crystal surfaces via electrostatic interactions (Cardoso et al., 2011). Furthermore, electrosprayed whey protein isolate/lactose nanocomposite capsules loaded with Lactobacillus acidophilus LA5 have shown smooth and uniform morphology (Amiri et al., 2021). However, these systems primarily exhibited crystalline or capsule-like structures rather than uniformly spherical amorphous particles. Moreover, the reported studies remain at the level of formulation development, with minimal exploration of their therapeutic functions.

To the best of our knowledge, this is the first study to develop electrosprayed lactose-based particles specifically for antibacterial applications. In this work, we aimed to fabricate cipro-loaded amorphous spherical lactose particles using electrospraying, and systematically evaluated their morphology, physicochemical characteristics, and, crucially, their antibacterial efficacy. Notably, we employed isothermal microcalorimetry to monitor bacterial growth inhibition in real time—this is a sensitive and underutilized technique in this context. This study thus bridges the gap between formulation design and functional performance evaluation, offering a novel approach to localized antimicrobial therapy. To prepare particles, lactose monohydrate (LM) was

* Corresponding author.
E-mail address: g.williams@ucl.ac.uk (G.R. Williams).

https://doi.org/10.1016/j.ijpharm.2025.125748
Received 11 April 2025; Received in revised form 13 May 2025; Accepted 20 May 2025
Available online 22 May 2025

combined with PVA, a polymer suitable for drug delivery owing to its non-toxic properties (Rytting et al., 2008). PVA plays a pivotal role as a helper polymer, significantly augmenting the electrospinnability of lactose.

2. Materials and methods

2.1. Materials

Materials were obtained as follows: ciprofloxacin (cipro, Fisher Scientific); poly(vinyl alcohol) (PVA, MW 30000 Da, Merck), *Pseudomonas aeruginosa* (NCTC 10662, Sigma-Aldrich); *Staphylococcus aureus* (WDCM 00,032 Vitroids, Sigma-Aldrich); lactose monohydrate (LM, $C_{12}H_{22}O_{11}{\cdot}H_2O$, Fisher Scientific); phosphate buffered saline (PBS) tablets (Sigma-Aldrich); acetic acid (AA, $\geq$ 99.7 %, Fisher Scientific); HCl (36.5 %-38 %, Sigma-Aldrich); ethanol ($\geq$ 99.8 %, Sigma-Aldrich); glycerol (Fisher Scientific); tryptic soy agar (TSA, Fisher Scientific); tryptic soy broth (TSB, Fisher Scientific); deionized water (Purite, Triple Red Limited, UK).

2.2. Electrospraying

Initially, LM and PVA were dissolved in a solvent blend at 90 °C and cooled to room temperature. A range of concentrations of LM, ratios of LM: PVA, and solvents were explored. The final electrosprayed formulation comprised 40 % w/v solute (LM: PVA = 9:1 w/w) in a water: ethanol: AA mixture at 80:5:15 v/v/v. Once the final recipe was determined, cipro at different concentrations was added to the formulation. The final drug concentrations were 0.25, 0.5, 0.75, 1, and 1.25 wt% cipro (with respect to the total weight of LM and PVA).

Solutions were electrosprayed with a 1 ml syringe (BD Plastipak), fitted with a 20G needle (0.337 mm nominal inner diameter, Nordson EFD). The distance between tip and collector was 16 cm. The flow rate was 0.1 ml/h. The voltage applied for the blank formulation was 13.28 kV, and that applied for the cipro-loaded formulations was 13.92 kV. The temperature was 20–25 °C and relative humidity 30 %-40 %. Materials were collected on a Teflon-coated metal plate.

2.3. Characterization

2.3.1. Scanning electron microscopy (SEM)

The morphology of the ES particles was identified using a Phenom Pro bench-top SEM (Thermo Fisher Scientific). Prior to imaging, the samples were sputter-coated with a thin layer of graphite to enhance conductivity. To ensure a representative analysis, 200 particles per formulation were randomly selected from multiple images and analyzed using the ImageJ 1.52a software. Particle size data are reported as mean ± standard deviation (SD), and the size distribution profiles were generated using Origin 2022b.

2.3.2. X-ray diffraction (XRD)

XRD was performed to characterize the physical form of the samples. The analysis was conducted using a Rigaku Miniflex 600 diffractometer equipped with Cu Kα radiation ($\lambda = 1.5418$ Å), operating at 40 kV and 15 mA. Diffraction patterns were recorded over a 2θ range of 3° to 40° with a scan rate of 5°/min.

2.3.3. Fourier-transform infrared spectroscopy (FTIR)

FTIR spectra were acquired using a PerkinElmer Spectrum 100 spectrometer. Each spectrum was collected over the range of 4000–650 cm^{-1} with a resolution of 1 cm^{-1}, averaging four scans per measurement.

2.3.4. Thermogravimetric analysis (TGA)

Thermal stability and weight loss profiles of the formulations were assessed using a TA Instruments Discovery TGA system. Samples were gradually heated from 40 °C to 500 °C at a rate of 10 °C/min under a controlled nitrogen flow of 25 ml/min. The acquired data were processed using TA Trios software.

2.3.5. Differential scanning calorimetry (DSC)

The thermal behavior of the samples was analyzed via DSC using a Q2000 DSC instrument. Nitrogen gas was used as the purge gas at a flow rate of 50 ml/min. The heating rate was set to 10 °C/min, with the temperature range determined based on TGA results to prevent sample degradation during the experiment.

2.3.6. Drug loading determination

To quantify the cipro content in the ES formulations, 5 mg of each sample was dissolved in 10 ml of 0.1 M HCl and incubated at 37 °C under continuous stirring overnight (Liu et al., 2025). The resulting suspensions were centrifuged at 10000 rpm for 10 min, and the supernatant was analyzed for cipro concentration using a Spectramax M2e UV–visible spectrophotometer (Molecular Devices) at 277 nm. A calibration curve for cipro in 0.1 M HCl was established over the range of 0.5–15 μg/ml ($R^2 = 0.9999$). The cipro content and entrapment efficiency were calculated using the equations below:

$$\textit{Cipro content}\ (\%) = (\textit{Mass of cipro in particles}/\textit{total mass of particles}) \times 100 \quad (1)$$

$$\textit{Entrapment efficiency}(\%) = (\textit{Measured cipro content}/\textit{theoretical content}) \times 100 \quad (2)$$

2.3.7. Drug release

In vitro drug release studies were performed using a dialysis method, as described in our previous work (Liu et al., 2025). Precisely weighed ES samples were sealed in dialysis tubing (BioDesign, 3500 MWCO, Fisher Scientific) and immersed in 200 ml of PBS (pH 7.4). The system was kept at 37 °C with gentle shaking at 50 rpm. The amount of sample used for each formulation was adjusted to ensure that the maximum cipro concentration remained below 5 μg/ml, calculated based on drug loading data.

At predetermined intervals over a 24 h period, 2 ml of the release medium was withdrawn and replaced with an equal volume of fresh preheated PBS. The aqueous solubility of cipro is documented as 30 mg/ml at 20 °C and pH 11, the selected experimental concentration (5 μg/ml) was approximately 6000-fold lower than the solubility limit (Liu et al., 2025). The collected samples were analyzed at 270 nm using a Spectramax M2e instrument, with cipro concentrations determined via a pre-established calibration curve in PBS (0.5–15 μg/ml, $R^2 = 0.9994$).

The percentage of cumulative drug release was calculated relative to the initial drug content in the particles. The data were collected from three separate experiments and presented as mean ± SD.

2.3.8. Antibacterial activity of cipro-loaded ES particles

Bacterial culture of *P. aeruginosa* and *S. aureus*, as well as the antibacterial efficacy of cipro were described in our previous work (Liu et al., 2025). Initially, a bacteria pellet was suspended in 1 ml of TSB (first generation), vortexed, and then transferred to 40 ml of TSB for incubation at 37 °C for 24 h. After incubation, the culture was vortexed, and 1 ml of the resultant culture was transferred to 40 ml of fresh TSB for subculture (second generation). Then, 5 ml of the overnight culture was added to 250 ml of fresh TSB broth and incubated at 37 °C. After vortexing, a 1 ml sample was withdrawn, vortexed, and its optical density (OD) was measured at 600 nm using a spectrophotometer (CO8000 cell density meter, WPA Biowave). When the OD reading reached between 0.4–0.7 (indicative of the exponential growth phase), the culture was processed for freezing.

For freezing, 0.1 ml of the culture suspension was mixed with 0.9 ml of PBS in sterile tubes and labeled as 10^{-1}. The solution was then serially diluted in tenfold increments, generating dilutions ranging from 10^{-2} to 10^{-7}. Then, 50 µl from each dilution was plated onto TSA plates and spread with a fresh spreader. After incubation for 24 h, plates with a countable number of colonies (2–300 colonies) were selected, and the colonies were counted to determine the colony-forming units per milliliter (CFU/ml). The procedure was repeated three times for each dilution. The final inoculum concentration was determined to be 10^8 CFU/ml for both *P. aeruginosa* and *S. aureus*.

The remaining liquid culture (OD reading between 0.4–0.7) was centrifuged at 9500 rpm at 4 °C for 10 mins to collect a bacteria pellet. The supernatant was carefully discarded, and the resultant pellet was thoroughly resuspended in PBS, followed by centrifugation. This PBS resuspension and centrifugation procedure was repeated three times. The pellet was then resuspended in 20 % glycerol (v/v), aliquoted into 2 ml cryovials, and stored at −80 °C. Throughout the process, vortexing was performed, and TSA plates were prepared to ensure purity, with no signs of contamination.

The minimum heat inhibitory concentration (MHIC) of free cipro against *P. aeruginosa* and *S. aureus* was determined *in vitro* using isothermal calorimetry, as described in the previous work (Liu et al., 2025). The MHIC was defined as the minimum concentration of antibiotic that did not produce heat flow in the calorimeter over 24 h. To prepare the cipro stock solution, free cipro was dissolved in 200 ml of 0.5 % v/v aqueous acetic acid to achieve a concentration of 1000 µg/ml. Dilutions were then made to obtain concentrations of 100 µg/ml, 10 µg/ml, and 1 µg/ml by further diluting the stock solution with sterile water and filtering through a 0.22 µm filter. Separate cipro solutions were prepared for *P. aeruginosa* and *S. aureus* (see Supporting Information, Tables S1 and S2) (Liu et al., 2025). For the isothermal calorimetry experiment, 2 ml of TSB (37 °C), cipro solution, and sterile water were pipetted into a 3 ml calorimetric ampoule (glass). A 0.03 ml of bacterial culture was added, achieving a total volume of 3 ml. The ampoule was sealed, vortexed, and equilibrated for 30 min at 37 °C in a Thermal Activity Monitor (TAM, TA Instruments Ltd.). Data were recorded using the Digitam 4.1 software (amplifier setting: 3000 µW) and presented as curves of heat flow (µW) vs. time (h). Control groups consisted of *P. aeruginosa* or *S. aureus* without cipro. Each concentration was tested in triplicate, and the resulting curves were either overlapping or very close to each other, with a single representative dataset presented. The inoculum size was 10^6 CFU/ml.

The MHIC values of ES particles against *P. aeruginosa* and *S. aureus* were also evaluated using isothermal calorimetry (Liu et al., 2025). Stock solutions of the particles at concentrations of 1000, 100, and 10 µg/ml were prepared and filtered through a 0.22 µm filter. For the calorimetric assay, 2 ml of TSB (37 °C), bacterial inoculum (0.03 ml), particle stock suspension, and water were added to calorimetric ampoules, with a total volume of 3 ml. The ampoules were then processed as described previously (Liu et al., 2025). Control groups consisted of pure *P. aeruginosa* or *S. aureus*, and a blank formulation (40 % w/v LM: PVA = 9:1 w/w in water: ethanol: AA = 80:5:15 v/v/v). Four different concentrations of ES particles were tested for each formulation, and each concentration was analyzed in triplicate. The resulting curves were either overlapping or very close to each other, so only one representative dataset is reported. The results from isothermal calorimetry are presented as heat flow (µW) vs. time (h). The bacterial inoculum size was 10^6 CFU/ml.

3. Results

3.1. Fabrication of ES particles

3.1.1. Initial optimization

It was found that LM alone could not be processed into solid particles by ES. Thus, PVA was introduced as a supplementary polymer to enhance the processability of LM (Jatal et al., 2021). Using water alone as the solvent, we observed that the cone-jet mode was not stable. A stable cone-jet is vital for particle formation, and influenced by several parameters including conductivity, viscosity, collection distance, flow rate, voltage, and solvent composition (Bock et al., 2012). Stabilizing the jet necessitated co-solvent addition. Consequently, subsequent work utilized acetic acid (AA) and ethanol for enhanced stability. After optimization, the solvent system was finally set as water: ethanol: AA at a ratio of 80:5:15 v/v/v. As depicted in Fig. 1, utilizing 40 % w/v LM: PVA = 9:1 w/w in water: ethanol: AA = 80:5:15 v/v/v yields spherical particles, with a mean particle size of 1.43 ± 0.45 µm. This formulation was deemed optimal for further experimentation.

3.1.1.1. Variation of drug loading. The drug concentrations tested were 0.25, 0.5, 0.75, 1, 1.25 wt% cipro (with respect to the total weight of LM and PVA). SEM images are given in Fig. 2a-e, and reveal that the ES particles exhibit a consistently smooth surface and spherical morphology. They also display a uniform size distribution, albeit with varying degrees of particle aggregation, which is typical for particles falling within the 1–5 µm size range. Additionally, it is also found that varying the cipro content does not markedly alter the particle size or size distribution (Fig. 2f, Table 1). All the ES formulations exhibit mean diameters around 1.30 – 1.80 µm.

3.2. Characterization of ES particles

3.2.1. XRD

XRD patterns for the ES particles are displayed in Fig. 3. Raw cipro and LM exhibit crystalline characteristics, evident from the sharp Bragg reflections in the diffraction patterns. All the ES particles present diffuse haloes, signifying the absence of crystalline LM or cipro formation after drying. These findings suggest that cipro and LM underwent conversion into the amorphous physical form through electrospraying. This aligns with findings in the literature (Jaworek and Sobczyk, 2008; Wang et al., 2012). It should be noted however that the drug loading is low here, and so caution must be taken as the limit of detection of the instrument could make it challenging to detect crystalline cipro.

3.2.2. FT-IR

The IR spectra of the ES particles are depicted in Fig. 4. In the PVA spectrum, the absorption band between 3424 and 3093 cm^{-1} is attributed to the O–H groups, whereas the band at 2916 cm^{-1} corresponds to the symmetrical stretching vibration of C–H within the PVA backbone. Additionally, secondary in-plane O–H bending is observed at 1426 cm^{-1} (Silva et al., 2018).

In the LM spectrum, a sharp, distinct, O–H stretch observed at 3529 cm^{-1} suggests constrained water in the crystal lattice. This cannot be observed in the spectra of the formulations, indicating the absence of water in a crystal lattice and consistent with the amorphous nature of the materials indicated by XRD (Buckton et al., 1998). The absorption band ranging from 3382 to 2983 cm^{-1} is attributed to O–H stretching, while the peak at 1655 cm^{-1} represents the delta bend of water (Ottenhof et al., 2003). The absorption bands at 2936 cm^{-1} and 2899 cm^{-1} correspond to the symmetric stretching vibration and the asymmetric stretching vibration of the CH_2 groups in lactose (Wiercigroch et al., 2017). Furthermore, the distinctive doublet peaks at 1036 and 1022 cm^{-1} represent C–C stretching (Madžarević et al., 2021). Additionally, the band between 1200–1060 cm^{-1} is assigned to the asymmetric stretching vibration of C-O-C in glucose and galactose. In the spectrum of cipro, the bands at 3043 and 2851 cm^{-1} correspond to the C–H stretching vibration from the phenyl ring, while distinct peaks at 1585 and 1542 cm^{-1} result from benzene ring stretching vibrations and that at 1612 cm^{-1} is the C=O stretch (Pandey et al., 2012; Türeli et al., 2017; Dillen et al., 2006).

For the ES formulations, the broad stretching band from 3600 to

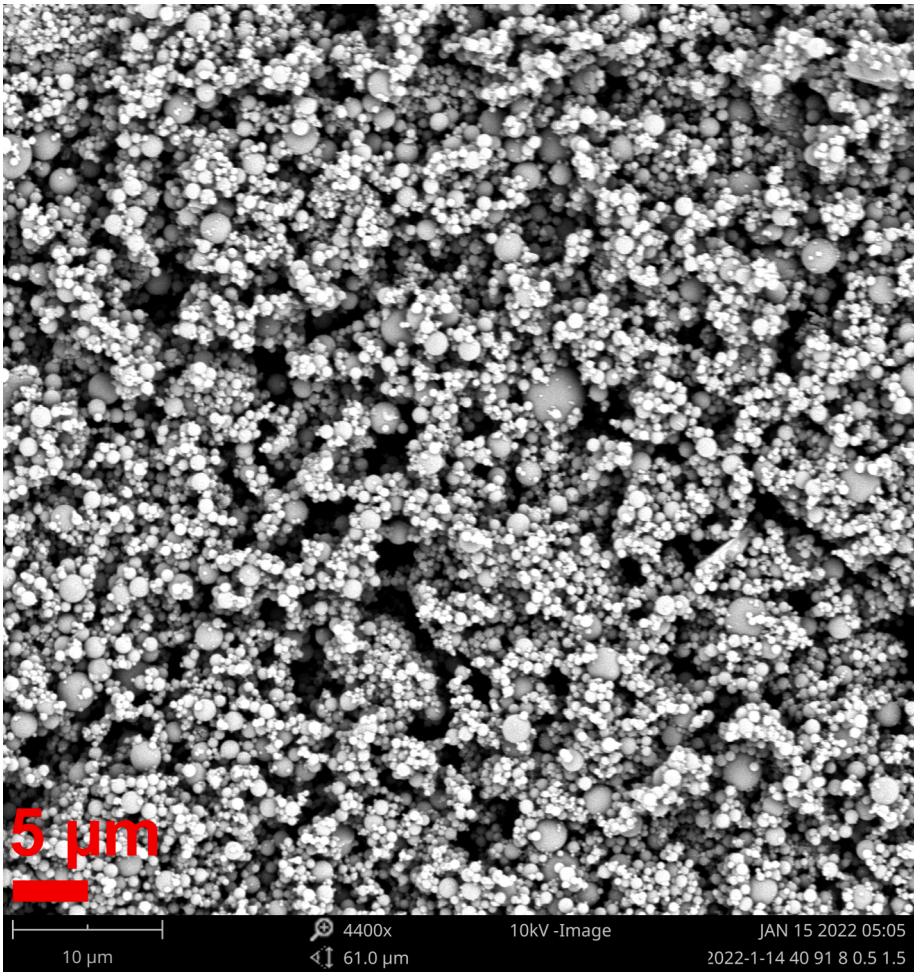

Fig. 1. SEM image of particles prepared with 40 % w/v solute, LM: PVA = 9:1 w/w, water: ethanol: AA = 80:5:15 v/v/v.

3000 cm^{-1} is attributed to the O–H groups of LM and PVA. The band at 2910 cm^{-1} might arise from the overlapping symmetrical C–H stretching vibration of the PVA backbone and the CH_2 group vibrations in lactose. The band from 1100 cm^{-1} to 1000 cm^{-1} might reflect the coexistence of carbohydrate and OH structures in both materials. Distinct characteristic peaks of cipro can be observed in the particles, including the C=O stretching vibration at 1612 cm^{-1} (Pandey et al., 2012), the benzene ring stretching at 1585 cm^{-1} (Türeli et al., 2017), and the aromatic C=C stretching at 1542 cm^{-1} (Dillen et al., 2006). However, these peaks appear with reduced intensity and slight peak shifts, which can be attributed to potential hydrogen bonding or the molecular interactions between cipro and the PVA/LM matrix.

3.2.3. Thermal analysis

TGA curves (Fig. S1) of the ES particles demonstrate weight loss trends akin to LM. The initial weight loss, occurring between 50–130 °C, is attributed to water loss. For the ES formulations, water loss ranged from 6 % to 8 %. This relatively high value can be attributed to the use of water in the ES solvent system and the fabrication, storage, and handling of the samples under atmospheric conditions (Peltonen et al., 2010). Additionally, the slow electrospraying process, conducted at room temperature (RH ~ 30–40 %), along with the hygroscopic nature of PVA, may have contributed to the higher moisture content.

The second weight loss is attributed to decomposition of the formulations. For all ES formulations, decomposition processes all commence at around 180 °C, possibly due to the small differences in drug contents. However, the decomposition of the formulations starts earlier compared to the raw materials. This can be attributed to the amorphous nature of the formulations, which facilitates easier molecular movement and degradation, unlike the crystalline raw materials where a lattice enthalpy barrier impedes molecular motion (Yu et al., 2018).

The DSC curves of the ES particles are given in Fig. S2. The ES formulations exhibit shallow and broad endotherms in the range of 30–70 °C, attributed to the loss of water (Ping et al., 2001). This is consistent with the TGA results. Determining the physical form of cipro in the formulations based on the DSC data is not possible since the DSC traces were stopped before reaching the melting temperature of cipro, and additionally the drug content is low.

3.2.4. Drug loading

As outlined in Table 2, the highest w/w drug loading of the ES particles is 1.07 %. For the formulations with relatively higher loadings (0.5 %, 0.75 %, 1 %, 1.25 % wt. cipro), the encapsulation efficiency (EE) values are below 100 %, possibly due to precipitation of drug in the syringe, or deposition of material elsewhere than on the collector. This phenomenon aligns with previous studies, which have reported a decline in EE at higher drug concentrations, likely attributed to phase separation or insufficient drug-polymer interactions during the electrospraying process (Das et al., 2010; Keawchaoon and Yoksan, 2011; Uyen et al., 2020).

3.2.5. Drug release

The results of dissolution tests, presented in Fig. 5, reveal similar release profiles with all the ES particles, with rapid drug release occurring within 5 h. These relatively fast rates may be partly attributed

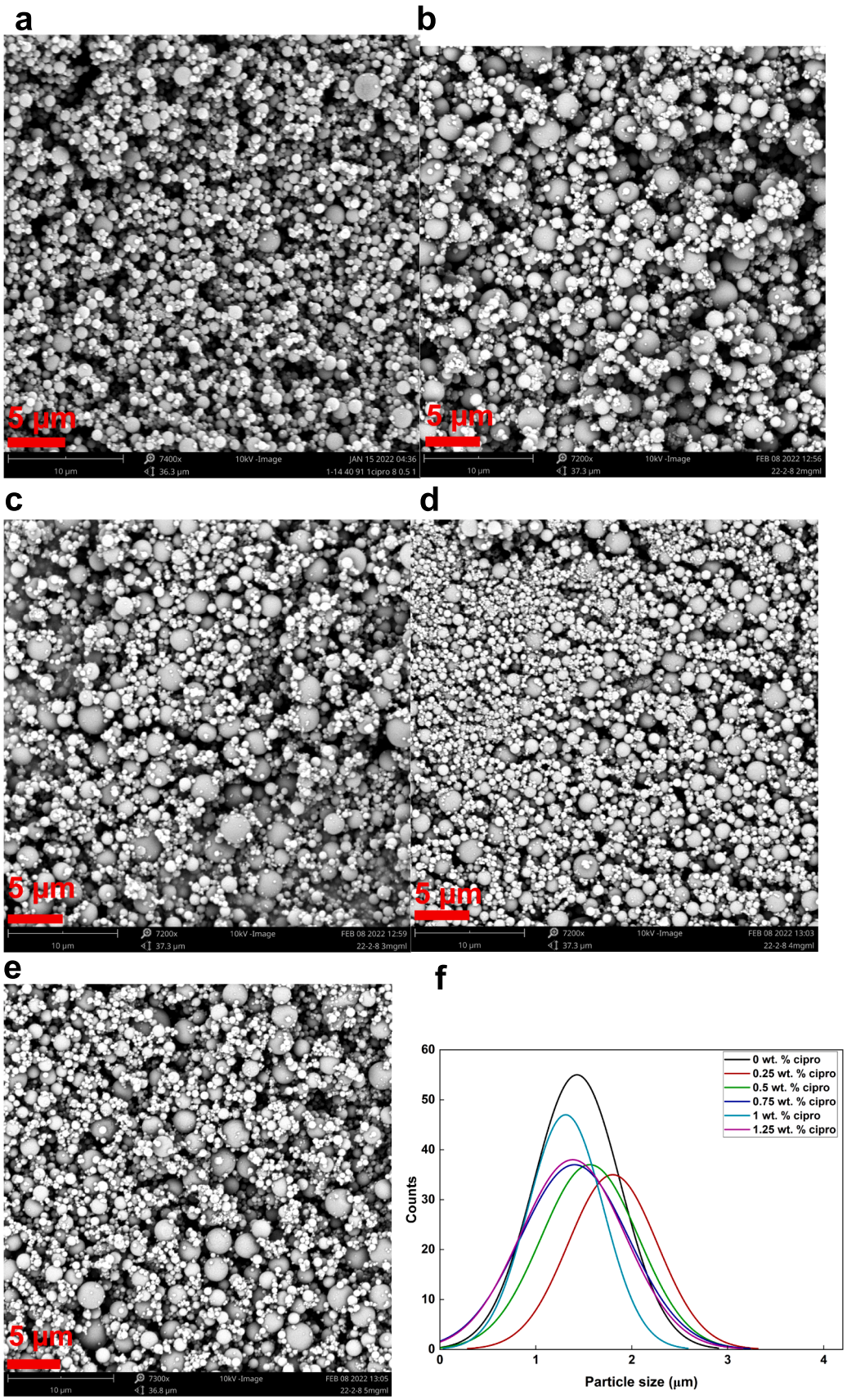

Fig. 2. SEM images for **(a)** 0.25, **(b)** 0.5, **(c)** 0.75, **(d)** 1, and **(e)** 1.25 wt% cipro loaded particles (40 % w/v, LM: PVA = 9:1 w/w, water: ethanol: AA = 80:5:15 v/v/v) together with (**f**) size distribution curves.

Table 1
The sizes of the cipro-loaded ES particles.

Formulation	Mean particle size (μm)
0 wt% cipro	1.43 ± 0.45
0.25 wt% cipro	1.80 ± 0.47
0.5 wt% cipro	1.56 ± 0.51
0.75 wt% cipro	1.40 ± 0.56
1 wt% cipro	1.31 ± 0.39
1.25 wt% cipro	1.39 ± 0.54

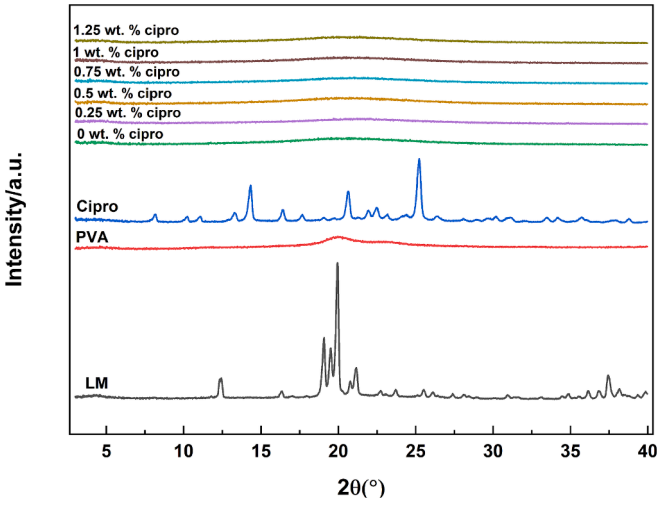

Fig. 3. XRD patterns of the raw materials and ES particles.

to the sink conditions employed in this setup. It is found that the ES formulations release the majority of their cipro cargo (74 %-91 %) over 24 h. However, the ES particles cannot release 100 % of their drug loading. The cause of the incomplete release may be strong interactions between the drug and PVA and/or LM.

3.2.6. *Antibacterial activity of ES particles*

The MHIC values of cipro-loaded ES particles against *P. aeruginosa* and *S. aureus* were determined by isothermal microcalorimetry. The antibacterial effect of cipro alone was determined in our previous work to be an MHIC of 0.5 μg/ml for *P. aeruginosa* and 0.8 μg/ml for *S. aureus* (Fig. S3 and Fig. S4) (Liu et al., 2025). Both *P. aeruginosa* and *S. aureus* exhibit "sensitivity" to the blank formulation (40 % w/v, LM: PVA = 9:1 w/w, water: ethanol: AA = 80:5:15 v/v/v) at a concentration of 1000 μg/ml. For *P. aeruginosa*, the elevated heat production observed with the blank formulation indicates enhanced bacterial growth, possibly due to the nutrient-rich lactose present in the particles, which supports bacterial metabolism. Conversely, for *S. aureus*, the reduced heat production suggests inhibited bacterial growth, potentially caused by the antimicrobial effect of residual AA in the ES formulation. The presence of residual AA is suggested by TGA and DSC analyses. In the TGA profile, after the initial loss of free water (around 70–120 °C), a gradual and smooth mass loss is observed, which may correspond to the volatilization of residual AA. This is further supported by the DSC curve, where a subtle endothermic peak within the same temperature range provides additional evidence for the presence of residual AA.

However, this mild antibacterial effect of the blank formulation at high concentrations (1000 μg/ml) is unlikely to influence the interpretation of results for the cipro-loaded particles, which exhibited complete bacterial inhibition at much lower concentrations (≤200 μg/ml). The cipro in the ES formulations retains its antibacterial efficacy, as evidenced by the concentration-dependent delayed growth of both *P. aeruginosa* and *S. aureus* compared to the control bacterial growth curve (GC) (Fig. 6, Fig. 7).

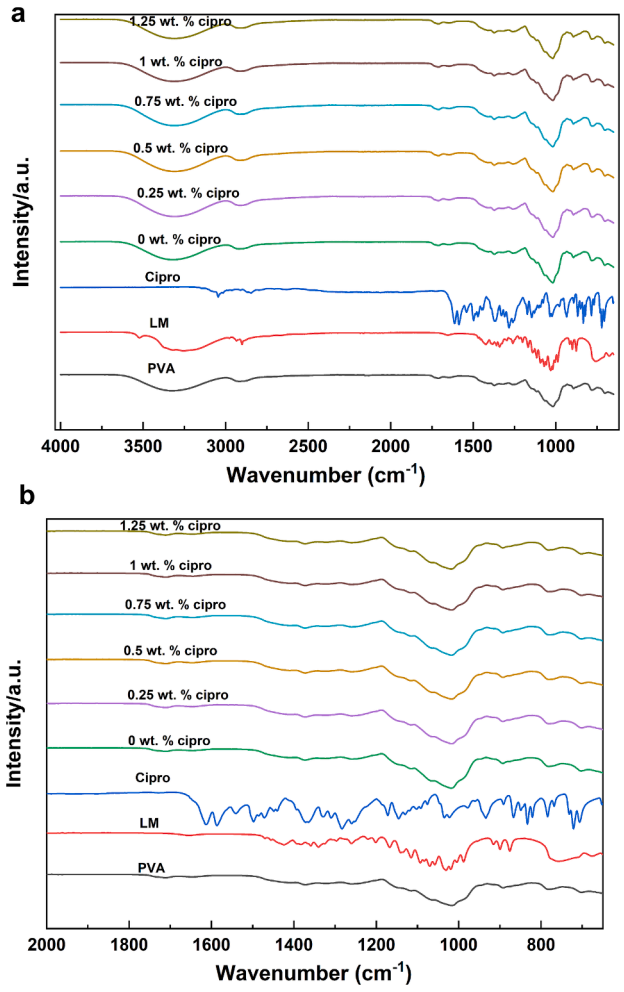

Fig. 4. (a) FT-IR spectra for the raw materials and ES particles and **(b)** an enlarged view of the region between 2000–650 cm^{-1}.

Table 2
Drug loading and EE of the ES particles.

ES particles	Drug loading (%)	EE (%)
0.25 wt% cipro	0.25 ± 0.01	101.9 ± 3.4
0.5 wt% cipro	0.45 ± 0.02	89.3 ± 3.1
0.75 wt% cipro	0.66 ± 0.02	88.3 ± 2.2
1 wt% cipro	0.87 ± 0.04	86.8 ± 4.1
1.25 wt% cipro	1.07 ± 0.02	85.3 ± 1.4

Once the concentration of the formulation reached the MHIC, no bacterial growth is observed. The MHIC values of cipro-loaded ES particles against *P. aeruginosa* and *S. aureus* are summarized in Table 4. Notably, ES formulations with higher drug loading exhibit lower MHIC values. Furthermore, the cipro-loaded ES formulations exhibit an antibacterial effect comparable to that of pure cipro, as indicated by comparing the MHIC values of cipro with the normalized MHIC values of the formulations (normalized to the cipro content). This demonstrates that electrospraying and the interactions between cipro and the carrier materials do not diminish its antimicrobial efficacy, consistent with previous research findings (Arauzo et al., 2021; Puleo et al., 2024). However, due to the low drug content, relatively high concentrations of ES formulations are necessary to completely inhibit bacterial growth.

4. Discussion

Numerous studies have highlighted the antimicrobial potential of ES

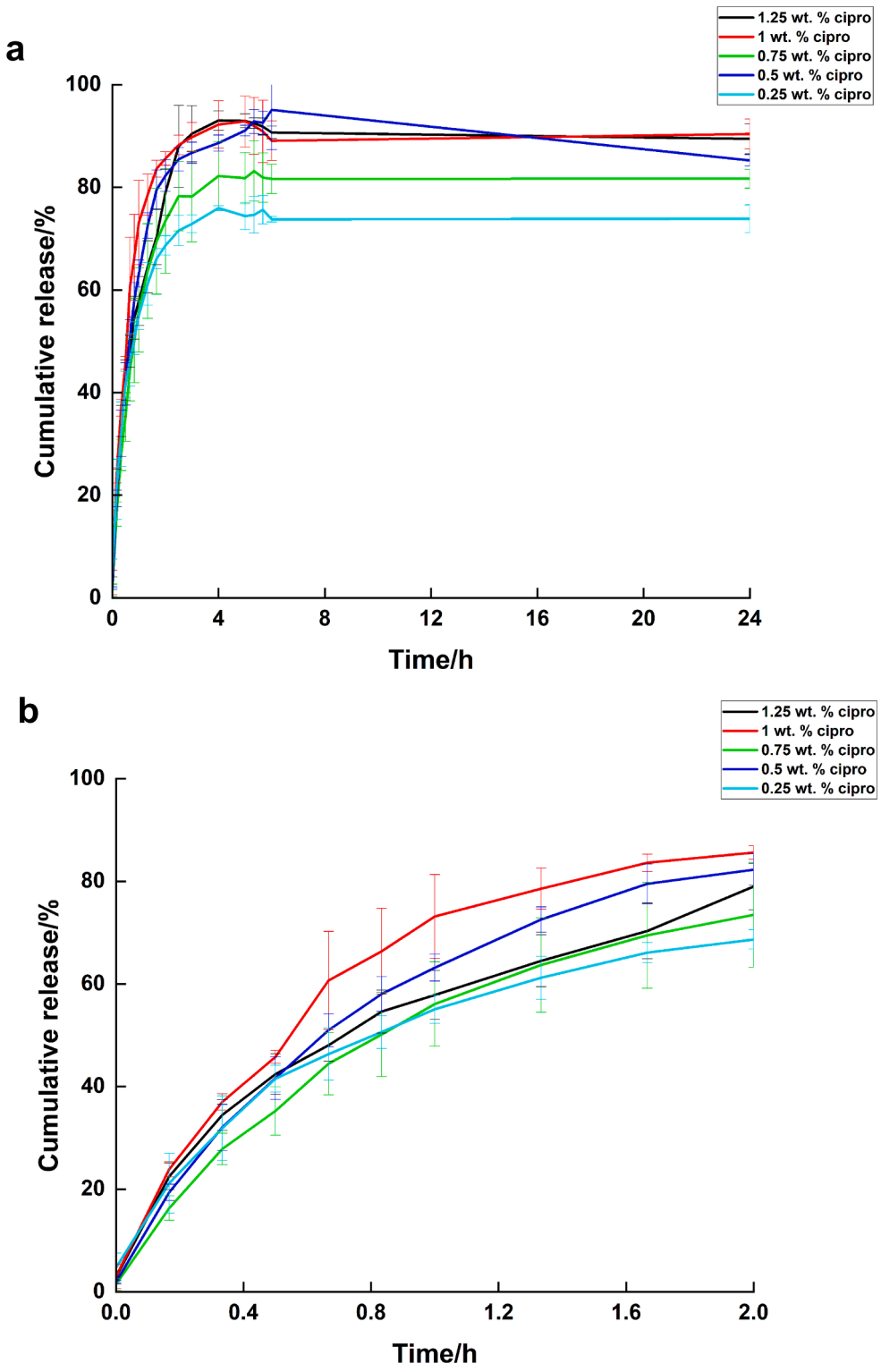

Fig. 5. **(a)** Release profiles of the ES particles (mean ± SD, n = 3). **(b)** Enlarged view of the first 2 h.

formulations. For example, ES vancomycin-loaded poly(lactic-co-glycolic acid) (PLGA) nanoparticles exhibited superior antibacterial activity against *S. aureus Xen 31* and *S. aureus Xen 36* compared to free vancomycin, attributed to improved interaction with bacterial cell walls and increased local drug concentration (Booysen et al., 2019). Similarly, ES azithromycin maintained comparable efficacy against *S. aureus* and *P. aeruginosa* while demonstrating cytocompatibility with human lung epithelial cell lines (A549 and Calu-3) at minimum inhibitory concentration doses (Arauzo et al., 2021). In addition, amoxicillin-loaded ES Eudragit RS sinking-magnetic microparticles (30 % Fe_3O_4) achieved superior eradication of *Helicobacter pylori in vivo* due to enhanced gastric retention (Hao et al., 2014). In another study, ES cipro loaded polybutylsuccinate microparticles effectively inhibited *P. aeruginosa* biofilm formation, showcasing the potential of electrospraying in tackling persistent infections (Puleo et al., 2024).

Nanofibres prepared by the sister electrospinning technique have

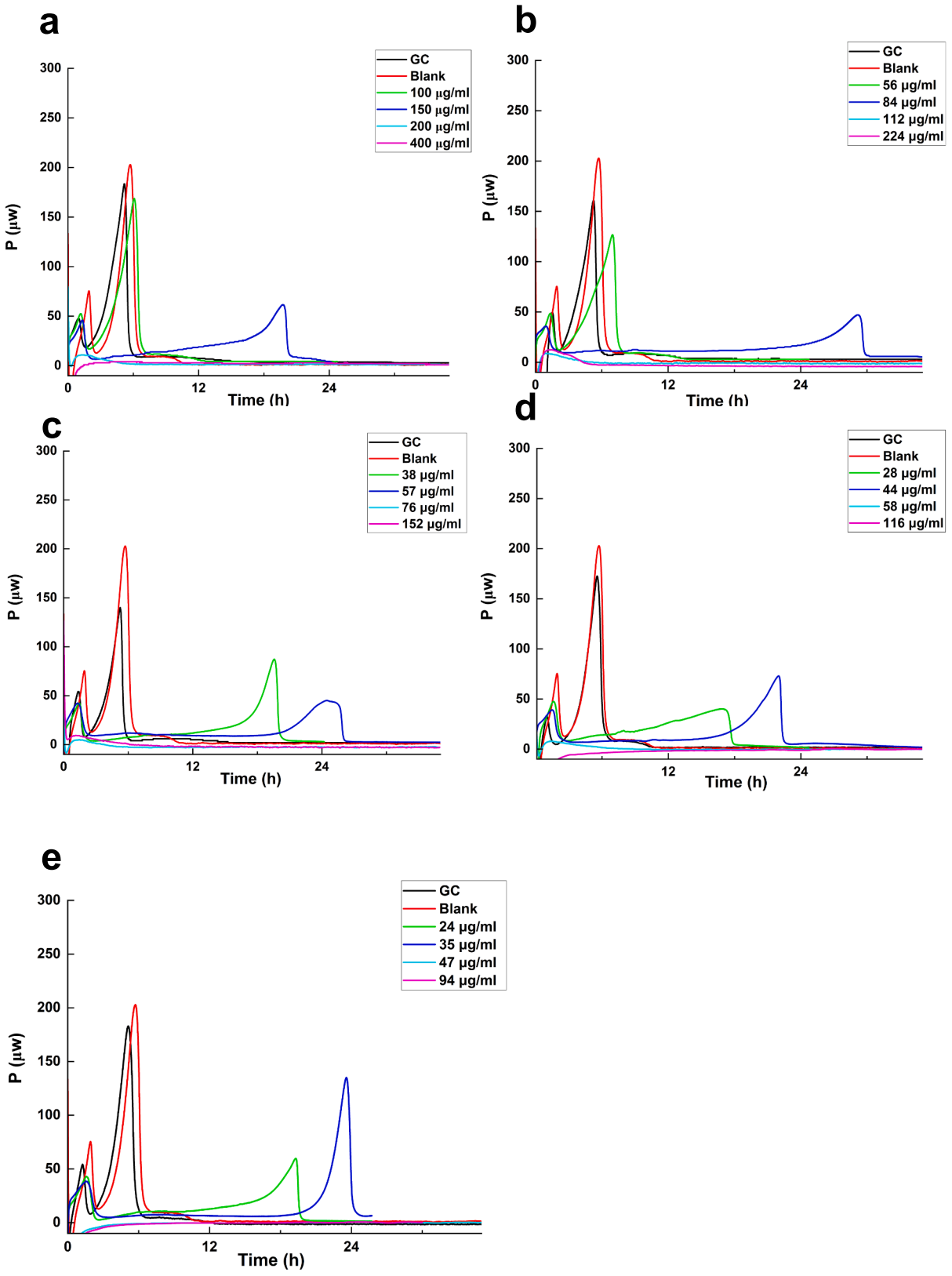

Fig. 6. Heat production (μW) vs time for *P. aeruginosa* incubated with the blank formulation (1000 μg/ml, 40 % w/v solute, LM: PVA = 9:1w/w, water: ethanol: AA = 80:5:15 v/v/v) and different concentrations of cipro-loaded ES particles with drug loadings of **(a)** 0.25 wt% **(b)** 0.5 wt% **(c)** 0.75 wt% **(d)** 1 wt% **(e)** 1.25 wt%. GC: untreated bacteria growth curve.

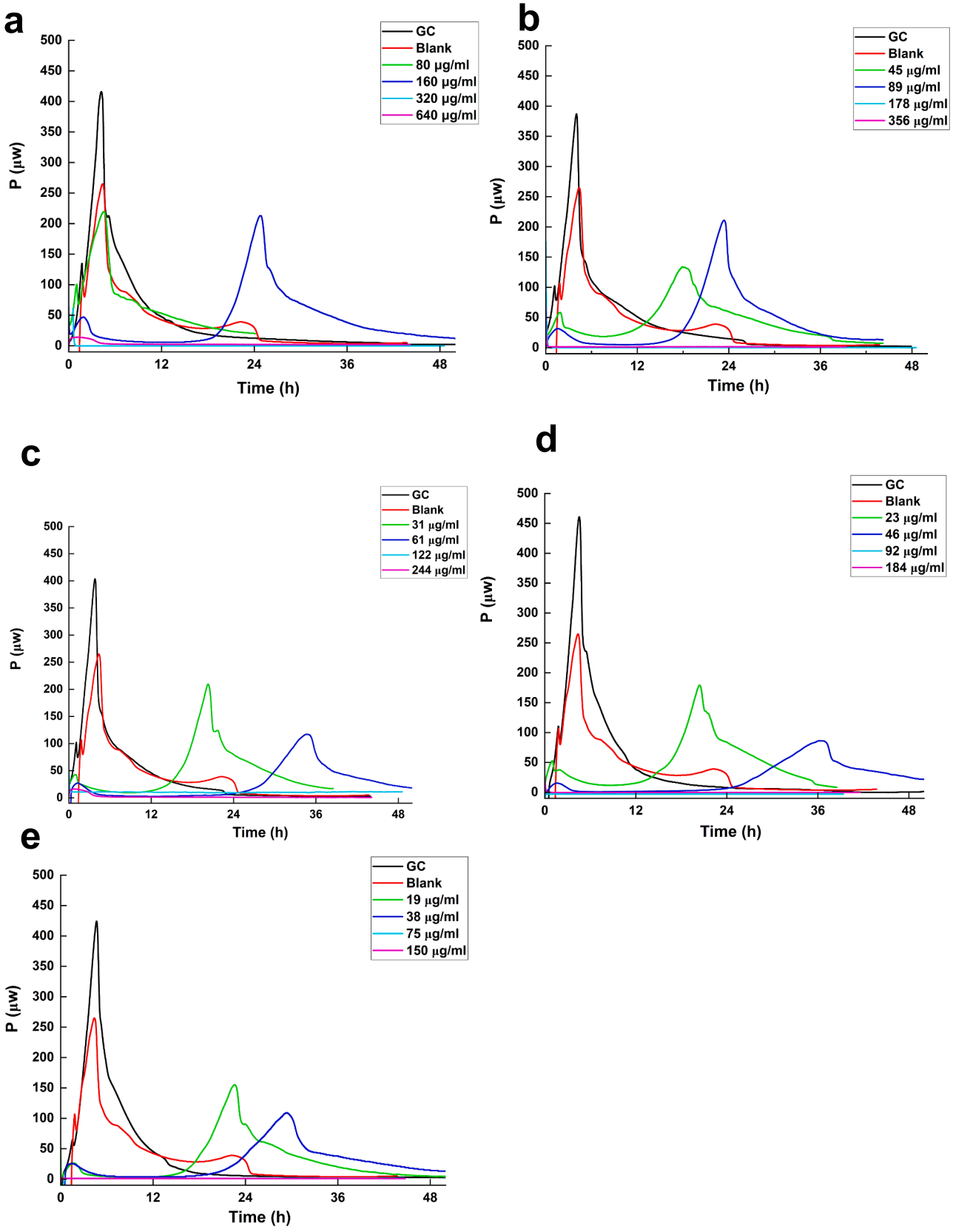

Fig. 7. Heat production (μW) vs time for *S. aureus* incubated with the blank formulation (1000 μg/ml, 40 % w/v solute, LM: PVA = 9:1w/w, water: ethanol: AA = 80:5:15 v/v/v) and different concentrations of cipro-loaded ES particles with drug loadings of **(a)** 0.25 wt% **(b)** 0.5 wt% **(c)** 0.75 wt% **(d)** 1 wt% **(e)** 1.25 wt%. GC: untreated bacteria growth curve.

Table 4
MHIC values of ES particles against *P. aeruginosa* and *S. aureus*.

Formulation	*P. aeruginosa*		*S. aureus*	
	MHIC of ES (μg particles/ml)	Normalized MHIC (μg cipro/ml)	MHIC of ES (μg particles/ml)	Normalized MHIC (μg cipro/ml)
0.25 wt% cipro	200	0.50	320	0.80
0.5 wt% cipro	112	0.50	178	0.80
0.75 wt% cipro	76	0.50	122	0.81
1 wt% cipro	58	0.50	92	0.80
1.25 wt% cipro	47	0.50	75	0.80

also been found to be potent. A novel hybrid material combining cipro polyvinylpyrrolidone (PVP) nanofibers with ES Ningmitai Eudragit S100 core–shell microparticles exhibited stronger antibacterial effects against *Escherichia coli (*E. coli*) dh5α* and *Bacillus subtilis Wb800* than the individual components (Sun et al., 2023). Similarly, rifampicin-loaded Eudragit RS100 fibers decorated with cipro-loaded Eudragit RS100 microparticles successfully eradicated both planktonic and biofilm forms of *E. coli* and *S. aureus*, with improved outcomes validated in a chronic infection mouse model (Miranda-Calderon et al., 2023).

Amoxicillin encapsulated in chitosan-hydroxyapatite composite matrices via electrospraying demonstrated antimicrobial effects against periodontal pathogens while exhibiting biocompatibility with gingival fibroblasts and osteoblasts (Zhang et al., 2025). Additionally, doxycycline-loaded ES PLGA microspheres exhibited activity against *Porphyromonas gingivalis* (Wang et al., 2019), while cefoxitin-loaded hyaluronic acid films targeted *S. aureus* Xen 36, *Klebsiella pneumoniae Xen 39*, and *Listeria monocytogenes EDGe* (Ahire and Dicks, 2016). Gramicidin-loaded ES poly(tetramethylene succinate) microparticles also displayed antibacterial activity against *E. coli* and *S. aureus* with excellent biocompatibility (Maione et al., 2016).

Electrospraying tetracycline-loaded particles onto titanium dioxide nanotubes within a PLGA matrix demonstrated antimicrobial activity against *S. aureus* while maintaining biocompatibility with MC3T3-E1 pre-osteoblast cells (Im et al., 2020). Cipro loaded chitosan submicron particles generated via electrospraying also showed potent activity against *S. aureus* and *P. aeruginosa*, with compatibility to alveolar cell lines (Arauzo et al., 2021). Furthermore, chlorogenic acid nanoparticles prepared in a PVA/PLGA matrix exhibited *in vivo* antibacterial effects against *P. aeruginosa* in a mouse lung infection model and antiviral activity against Human Coronavirus 229E and MERS-CoV (Saleh et al., 2023).

Through a series of optimization experiments, this study successfully developed cipro-loaded lactose particles via electrospraying. Unlike commercially available lactose particles Respitose® (SV003) (tomahawk crystals, 100 ± 2 μm) (Patil et al., 2017), and previously reported electrosprayed lactose particles (elongated crystals, 63–90 μm) (Patil et al., 2017), block-like lactose crystals (Cardoso et al., 2011), or microcapsule structures (~435 nm) (Amiri et al., 2021), the ES lactose particles developed in this study stand out due to their uniform, smooth, and spherical morphology (1–3 μm), along with their likely amorphous structure, potentially enhancing their functional properties.

Compared to cipro-loaded spray dried (SD) particles developed in previous research (Liu et al., 2025), though both the ES and SD formulations exhibited spherical morphology (ES: 1–3 μm; SD: 2–5 μm), and both processing methods successfully converted cipro and LM into the amorphous state, ES formulations exhibited a superior release profile, with 74–91 % of the cipro cargo being released more rapidly than the SD particles (70–80 %) over 24 h. The particle size difference between the SD and ES systems and presence of PVA in the latter likely contribute to these findings. The ES particles not only have smaller particle sizes (and hence a larger surface area), but also contained hydrophilic PVA (which was not included in the SD formulations); as a result, drug solubility and dissolution rate could be increased (Yu et al., 2018). These microparticles show potential for local application, particularly in the treatment of infections in the oral cavity and outer ear canal. This is further supported by previous studies, in which ES particles have shown promise in managing bacterial infections in these regions (Li et al., 2017; Park et al., 2023; Ibrahim et al., 2021; Cecchini et al., 2023).

Beyond the advantages in release kinetics, this study is the first to investigate the antibacterial performance of electrosprayed lactose particles using advanced isothermal microcalorimetry. This approach enabled real-time, dynamic, monitoring of bacterial metabolism in the presence of either free drug or formulated particles and allowed the determination of the MHIC for each formulation. The cipro-loaded ES lactose particles retained their antimicrobial efficacy and exhibited concentration-dependent antibacterial activity against *S. aureus* and *P. aeruginosa*, effectively delaying and inhibiting bacterial growth. These findings underscore the potential of ES lactose-based formulations as a promising approach for enhancing drug delivery efficiency and therapeutic effectiveness in combating bacterial infections.

5. Conclusions

In this work we successfully generated lactose monohydrate (LM)-based particles through electrospraying (ES) using PVA as an additive. ES particles were fabricated with various cipro loadings. SEM analysis confirmed the spherical morphology of the obtained particles. Both cipro and LM were thought to be transformed into the amorphous state during the electrospraying process. Additionally, it was observed that the ES particles contained residual water, primarily originating from the production process. The rapid drug release within 5 h indicates the potential of ES particles for local treatment of acute infections, for instance in the mouth and outer ear. Notably, the loaded cipro displayed concentration-dependent antibacterial activity against both *P. aeruginosa* and *S. aureus*, effectively delaying and inhibiting bacterial growth.

CRediT authorship contribution statement

Sai Liu: Writing – original draft, Visualization, Methodology, Investigation, Formal analysis, Data curation, Conceptualization. **Simon Gaisford:** Writing – review & editing, Resources, Methodology, Conceptualization. **Gareth R. Williams:** Writing – review & editing, Supervision, Resources, Data curation, Conceptualization.

Declaration of competing interest

The authors declare that they have no known competing financial interests or personal relationships that could have appeared to influence the work reported in this paper.

Appendix A. Supplementary data

Supplementary data to this article can be found online at https://doi.org/10.1016/j.ijpharm.2025.125748.

Data availability

Data will be made available on request.

References

Ahire, J.J., Dicks, L.M., 2016. Antimicrobial hyaluronic acid–cefoxitin sodium thin films produced by electrospraying. Curr. Microbiol. 73, 236–241.
Ali, A., Zaman, A., Sayed, E., Evans, D., Morgan, S., Samwell, C., et al., 2021. Electrohydrodynamic atomisation driven design and engineering of opportunistic

particulate systems for applications in drug delivery, therapeutics and pharmaceutics. Adv. Drug Deliv. Rev. 176, 113788.
Amiri, S., Teymorlouei, M.J., Bari, M.R., Khaledabad, M.A., 2021. Development of Lactobacillus acidophilus LA5-loaded whey protein isolate/lactose bionanocomposite powder by electrospraying: A strategy for entrapment. Food Biosci. 43, 101222.
Arauzo, B., Lopez-Mendez, T.B., Lobera, M.P., Calzada-Funes, J., Pedraz, J.L., Santamaria, J., 2021. Excipient-free inhalable microparticles of azithromycin produced by electrospray: a novel approach to direct pulmonary delivery of antibiotics. Pharmaceutics. 13 (12), 1988.
Arauzo, B., Lobera, M.P., Monzon, A., Santamaria, J., 2021. Dry powder formulation for pulmonary infections: Ciprofloxacin loaded in chitosan sub-micron particles generated by electrospray. Carbohydr. Polym. 273, 118543.
Bock, N., Dargaville, T.R., Woodruff, M.A., 2012. Electrospraying of polymers with therapeutic molecules: State of the art. Prog. Polym. Sci. 37 (11), 1510–1551.
Booysen, E., Bezuidenhout, M., van Staden, A.D.P., Dimitrov, D., Deane, S.M., Dicks, L. M., 2019. Antibacterial activity of vancomycin encapsulated in Poly (DL-lactide-co-glycolide) nanoparticles using electrospraying. Probiotics Antimicrob. Proteins 11, 310–316.
Buckton, G., Yonemochi, E., Hammond, J., Moffat, A., 1998. The use of near infra-red spectroscopy to detect changes in the form of amorphous and crystalline lactose. Int. J. Pharm. 168 (2), 231–241.
Cardoso, M.T., Talebi, M., Soares, P., Yurteri, C., Van Ommen, J., 2011. Functionalization of lactose as a biological carrier for bovine serum albumin by electrospraying. Int. J. Pharm. 414 (1–2), 1–5.
Cecchini, B., Rovelli, R., Zavagna, L., Azimi, B., Macchi, T., Kaya, E., et al., 2023. Alginate-based patch for middle ear delivery of probiotics: a preliminary study using electrospray and electrospinning. Appl. Sci. 13 (23), 12750.
Das, R.K., Kasoju, N., Bora, U., 2010. Encapsulation of curcumin in alginate-chitosan-pluronic composite nanoparticles for delivery to cancer cells. Nanomed. Nanotechnol. Biol. Med. 6 (1), 153–160.
Dillen, K., Vandervoort, J., Van den Mooter, G., Ludwig, A., 2006. Evaluation of ciprofloxacin-loaded Eudragit® RS100 or RL100/PLGA nanoparticles. Int. J. Pharm. 314 (1), 72–82.
Eltohamy, M., Shin, U.S., Won, J.-E., Kim, J.-J., Kim, H.-W., 2011. Electrosprayed tricalcium phosphate spherical microcups and antibiotic drug delivery. Mater. Lett. 65 (13), 2043–2046.
Hao, S., Wang, Y., Wang, B., 2014. Sinking-magnetic microparticles prepared by the electrospray method for enhanced gastric antimicrobial delivery. Mol. Pharm. 11 (5), 1640–1650.
Hsu, Y.-H., Chen, D.-W.-C., Li, M.-J., Yu, Y.-H., Chou, Y.-C., Liu, S.-J., 2018. Sustained delivery of analgesic and antimicrobial agents to knee joint by direct injections of electrosprayed multipharmaceutical-loaded nano/microparticles. Polymers 10(8): 890.
Ibrahim, A., Moodley, D., Uche, C., Maboza, E., Olivier, A., Petrik, L., 2021. Antimicrobial and cytotoxic activity of electrosprayed chitosan nanoparticles against endodontic pathogens and Balb/c 3T3 fibroblast cells. Sci. Rep. 11 (1), 24487.
Im, S.-Y., Kim, K.-M., Kwon, J.-S., 2020. Antibacterial and osteogenic activity of titania nanotubes modified with electrospray-deposited tetracycline nanoparticles. Nanomaterials 10 (6), 1093.
Jatal, R., Osman, R., Mamdouh, W., Awad, G.A., 2021. Lung targeted electrosprayed chitosan nanocomposite microparticles boost the cytotoxic activity of magnolol. Carbohydr. Polym. Technol. Appl. 2, 100169.
Jaworek, A., Sobczyk, A.T., 2008. Electrospraying route to nanotechnology: An overview. J. Electrostat. 66 (3–4), 197–219.
Junkert, A.M., Lazo, R.E.L., Deffert, F., Carneiro, J., Borba, H.H.L., de Campos, M.L., et al., 2024. Pharmacokinetics of oral ciprofloxacin in adult patients: A scoping review. Br. J. Clin. Pharmacol. 90 (2), 528–547.
Keawchaoon, L., Yoksan, R., 2011. Preparation, characterization and in vitro release study of carvacrol-loaded chitosan nanoparticles. Colloids Surf. B Biointerfaces 84 (1), 163–171.
Kherroubi, L., Bacon, J., Rahman, K.M., 2024. Navigating fluoroquinolone resistance in Gram-negative bacteria: A comprehensive evaluation. JAC-Antimicrob. Resist. 6 (4), dlae127.
Landa, G., Alejo, T., Sauzet, T., Laroche, J., Sebastian, V., Tewes, F., et al., 2023. Colistin-loaded aerosolizable particles for the treatment of bacterial respiratory infections. Int. J. Pharm. 635, 122732.
Li, Y., Na, R., Wang, X., Liu, H., Zhao, L., Sun, X., et al., 2017. Fabrication of antimicrobial peptide-loaded PLGA/chitosan composite microspheres for long-acting bacterial resistance. Molecules 22 (10), 1637.
Liu, S., Gaisford, S., Williams, G.R., 2025. Ciprofloxacin-Loaded Spray-Dried Lactose Particles: Formulation Optimization and Antibacterial Efficacy. Pharmaceutics. 17 (3), 392.
Madžarević, M., Medarević, Đ., Pavlović, S., Ivković, B., Đuriš, J., Ibrić, S., 2021. Understanding the effect of energy density and formulation factors on the printability and characteristics of SLS Irbesartan tablets—Application of the decision tree model. Pharmaceutics. 13 (11), 1969.
Maione, S., del Valle, L.J., Pérez-Madrigal, M.M., Cativiela, C., Puiggali, J., Alemán, C., 2016. Electrospray loading and release of hydrophobic gramicidin in polyester microparticles. RSC Adv. 6 (77), 73045–73055.
Miranda-Calderon, L., Yus, C., de Ganuza, C.R., Paesa, M., Landa, G., Tapia, E., et al., 2023. Combinatorial wound dressings loaded with synergistic antibiotics in the treatment of chronic infected wounds. Chem. Eng. J. 476, 146679.
Naghavi, M., Mestrovic, T., Gray, A., Hayoon, A.G., Swetschinski, L.R., Aguilar, G.R., et al., 2024. Global burden associated with 85 pathogens in 2019: a systematic analysis for the Global Burden of Disease Study 2019. Lancet Infect. Dis. 24 (8), 868–895.
Naghavi, M., Vollset, S.E., Ikuta, K.S., Swetschinski, L.R., Gray, A.P., Wool, E.E., et al., 2024. Global burden of bacterial antimicrobial resistance 1990–2021: a systematic analysis with forecasts to 2050. Lancet 404 (10459), 1199–1226.
Nikolaou, M., Krasia-Christoforou, T., 2018. Electrohydrodynamic methods for the development of pulmonary drug delivery systems. Eur. J. Pharm. Sci. 113, 29–40.
Ottenhof, M.-A., MacNaughtan, W., Farhat, I.A., 2003. FTIR study of state and phase transitions of low moisture sucrose and lactose. Carbohydr. Res. 338 (21), 2195–2202.
Pandey, S., Pandey, P., Tiwari, G., Tiwari, R., Rai, A., 2012. FTIR spectroscopy: A tool for quantitative analysis of ciprofloxacin in tablets. Indian J. Pharm. Sci. 74 (1), 86.
Park, J.-E., Kim, Y.-K., Kim, S.-Y., Choi, J.-B., Bae, T.-S., Jang, Y.-S., et al., 2023. Biocompatibility and Antibacterial Effect of Ginger Fraction Loaded PLGA Microspheres Fabricated by Coaxial Electrospray. Materials. 16 (5), 1885.
Patil, S., Mahadik, A., Nalawade, P., More, P., 2017. Crystal engineering of lactose using electrospray technology: carrier for pulmonary drug delivery. Drug Dev. Ind. Pharm. 43 (12), 2085–2091.
Peltonen, L., Valo, H., Kolakovic, R., Laaksonen, T., Hirvonen, J., 2010. Electrospraying, spray drying and related techniques for production and formulation of drug nanoparticles. Expert Opin. Drug Deliv. 7 (6), 705–719.
Pilcer, G., Amighi, K., 2010. Formulation strategy and use of excipients in pulmonary drug delivery. Int. J. Pharm. 392 (1–2), 1–19.
Ping, Z., Nguyen, Q., Chen, S., Zhou, J., Ding, Y., 2001. States of water in different hydrophilic polymers—DSC and FTIR studies. Polymer 42 (20), 8461–8467.
Puleo, G., Terracina, F., Catania, V., Sciré, S., Schillaci, D., Licciardi, M., 2024. Electrosprayed Poly-butyl-succinate microparticles for sustained release of Ciprofloxacin as an antimicrobial delivery system. Powder Technol. 432, 119152.
Rytting, E., Nguyen, J., Wang, X., Kissel, T., 2008. Biodegradable polymeric nanocarriers for pulmonary drug delivery. Expert Opin. Drug Deliv. 5 (6), 629–639.
Saleh, A., Abdelkader, D.H., El-Masry, T.A., Eliwa, D., Alotaibi, B., Negm, W.A., et al., 2023. Antiviral and antibacterial potential of electrosprayed PVA/PLGA nanoparticles loaded with chlorogenic acid for the management of coronavirus and Pseudomonas aeruginosa lung infection. Artif. Cells Nanomed. Biotechnol. 51 (1), 255–267.
Silva, D.M., Paleco, R., Traini, D., Sencadas, V., 2018. Development of ciprofloxacin-loaded poly (vinyl alcohol) dry powder formulations for lung delivery. Int. J. Pharm. 547 (1–2), 114–121.
Steipel, R.T., Gallovic, M.D., Batty, C.J., Bachelder, E.M., Ainslie, K.M., 2019. Electrospray for generation of drug delivery and vaccine particles applied in vitro and in vivo. Mater. Sci. Eng. C 105, 110070.
Sun, L., Zhou, J., Chen, Y., Yu, D.-G., Liu, P., 2023. A combined electrohydrodynamic atomization method for preparing nanofiber/microparticle hybrid medicines. Front. Bioeng. Biotechnol. 11, 1308004.
Türeli, N.G., Torge, A., Juntke, J., Schwarz, B.C., Schneider-Daum, N., Türeli, A.E., et al., 2017. Ciprofloxacin-loaded PLGA nanoparticles against cystic fibrosis P. aeruginosa lung infections. Eur. J. Pharm. Biopharm. 117, 363–371.
Uyen, N.T.T., Hamid, Z.A.A., Tram, N.X.T., Ahmad, N., 2020. Fabrication of alginate microspheres for drug delivery: A review. Int. J. Biol. Macromol. 153, 1035–1046.
Wang, J., Helder, L., Shao, J., Jansen, J.A., Yang, M., Yang, F., 2019. Encapsulation and release of doxycycline from electrospray-generated PLGA microspheres: Effect of polymer end groups. Int. J. Pharm. 564, 1–9.
Wang, M., Rutledge, G.C., Myerson, A.S., Trout, B.L., 2012. Production and characterization of carbamazepine nanocrystals by electrospraying for continuous pharmaceutical manufacturing. J. Pharm. Sci. 101 (3), 1178–1188.
Wiercigroch, E., Szafraniec, E., Czamara, K., Pacia, M.Z., Majzner, K., Kochan, K., et al., 2017. Raman and infrared spectroscopy of carbohydrates: A review. Spectrochim. Acta A Mol. Biomol. Spectrosc. 185, 317–335.
Yu, D.-G., Li, J.-J., Williams, G.R., Zhao, M., 2018. Electrospun amorphous solid dispersions of poorly water-soluble drugs: A review. J. Control. Release 292, 91–110.
Zamani, M., Prabhakaran, M.P., Ramakrishna, S., 2013. Advances in drug delivery via electrospun and electrosprayed nanomaterials. Int. J. Nanomed. 2997–3017.
Zhang, B., Yan, S., Zhang, Y., Wu, Y., 2025. Optimizing locally delivered periodontitis therapy: Development of chitosan-hydroxyapatite-encapsulated drug via electrospraying. J. Appl. Polym. Sci. 142 (1), e56309.